TECHNICAL MEMORANDUM

X-337

DYNAMIC DIRECTIONAL STABILITY CHARACTERISTICS FOR A GROUP OF BLUNT REENTRY BODIES AT TRANSONIC SPEEDS

By Harleth G. Wiley, Robert A. Kilgore,
and Ernest R. Hillje

Langley Research Center
Langley Field, Va.

NATIONAL AERONAUTICS AND SPACE ADMINISTRATION

WASHINGTON

October 1960

M

NATIONAL AERONAUTICS AND SPACE ADMINISTRATION

TECHNICAL MEMORANDUM X-337

DYNAMIC DIRECTIONAL STABILITY CHARACTERISTICS FOR A GROUP OF BLUNT REENTRY BODIES AT TRANSONIC SPEEDS*

By Harleth G. Wiley, Robert A. Kilgore,
and Ernest R. Hillje

SUMMARY

Measurements were made of the transonic aerodynamic damping in yaw and oscillatory directional stability for models of a group of blunt, high-drag, reentry bodies of revolution. The models were oscillated approximately $\pm 2^{\circ}$ about the yaw axis for a range of reduced-frequency parameter, based on maximum model diameter, from 0.019 to 0.105. Tests were made at angles of attack of 0°, 5°, and 10° for a range of Mach number from 0.59 to 1.35. Reynolds number for the tests, based on maximum model diameter, varied from 1.8×10^6 to 5.6×10^6.

Results show that the damping in yaw was critically dependent upon body variables, such as front-face shape, shoulder radius, body slope, and base shape. Test Reynolds number and model surface condition often had a powerful influence on the measured damping. The effect of the test and model conditions on the oscillatory directional stability was less pronounced.

INTRODUCTION

Blunt, high-drag bodies of revolution designed for reentry into an atmosphere often have unpredictable aerodynamic characteristics, particularly near transonic speeds where mixed flows are present. Examples of these trends are the nonlinear static stability characteristics for blunt bodies reported in references 1 and 2. Since the aerodynamic damping of a reentry body can have significant effects on the motion as the body decelerates toward transonic speeds and since flow separation powerfully affects the static aerodynamic characteristics (for example, see ref. 1), tests to determine the dynamic stability of blunt reentry bodies were

deemed important. Transonic wind-tunnel tests of some of the directional dynamic stability characteristics of models of a group of high-drag reentry bodies were made, therefore, in the Langley transonic blowdown tunnel. The models were oscillated in yaw by using a sting-mounted, force-driven mechanism similar in principle to those described in references 3 and 4.

SYMBOLS

All aerodynamic coefficients in this report are based on the maximum diameter of the model as the reference dimension and are presented in the body system of axes with moments referred to the oscillation axis.

A	maximum cross-sectional area of model, $\pi\left(\frac{d}{2}\right)^2$, sq ft
d	maximum diameter of model, ft unless otherwise indicated
M	free-stream Mach number
R	Reynolds number based on d
r	angular velocity in yaw, $\partial\psi/\partial t$, radians/sec
$\dot{r}$	angular acceleration in yaw, $\partial^2\psi/\partial t^2$, radians/sec^2
t	time, sec
V	free-stream velocity, ft/sec
α	angle of attack, deg
β	instantaneous angle of sideslip ($\sin\beta = -\sin\psi\cos\alpha$), radians
$\dot{\beta}$	time rate of change of sideslip, $\partial\beta/\partial t$, radians/sec
ρ	free-stream mass density of air, $\frac{\text{lb-sec}^2}{\text{ft}^4}$
ψ	instantaneous angle of yaw, radians
ω	circular frequency, 2π(Frequency of oscillation), radians/sec; when used as a subscript, ω denotes data obtained by oscillation tests

C_n yawing-moment coefficient, $\frac{\text{Yawing moment}}{\frac{\rho V^2}{2} Ad}$

C_{n_r} yaw damping derivative, change in yawing-moment coefficient with change in yawing velocity, $\frac{\partial C_n}{\partial\left(\frac{rd}{V}\right)}$, per radian

$C_{n_{\dot{r}}}$ change in yawing-moment coefficient with variation in rate of change in yawing velocity, $\frac{\partial C_n}{\partial\left(\frac{\dot{r}d^2}{V^2}\right)}$, per radian

C_{n_β} static directional derivative, change in yawing-moment coefficient with variation in sideslip angle, $\left(\frac{\partial C_n}{\partial \beta}\right)_{\beta \to 0}$, per radian

$C_{n_{\dot{\beta}}}$ change in yawing-moment coefficient with variation in rate of change of sideslip angle, $\frac{\partial C_n}{\partial\left(\frac{\dot{\beta}d}{V}\right)}$, per radian

$\left(C_{n_r} - C_{n_{\dot{\beta}}} \cos \alpha\right)_\omega$ damping-in-yaw parameter, $\frac{-V(\text{Aerodynamic damping constant})}{\frac{\rho V^2}{2} Ad^2}$, per radian

$\left(C_{n_\beta} \cos \alpha + \left(\frac{\omega d}{V}\right)^2 C_{n_{\dot{r}}}\right)_\omega$ oscillatory directional-stability parameter, $\frac{\text{Aerodynamic spring constant}}{\frac{\rho V^2}{2} Ad}$, per radian

APPARATUS AND MODELS

The tests were made in the Langley transonic blowdown tunnel which has a slotted, octagonal test section with 26 inches between flats. A more complete description of the tunnel is given in reference 5. The tests were made with a sting-mounted, hydraulically driven, oscillating mechanism which maintains a single-degree-of-freedom angular yawing

oscillation of the model while measurements are made of the moment required to maintain the known oscillation. The models are rigidly forced to oscillate and the measured moments are unaffected by random disturbances such as airstream turbulence and buffeting. The process is similar in principle to that described in references 3 and 4. A schematic representation of the oscillating model system with its mechanical and electrical components and a photograph of the oscillating mechanism are shown in figure 1. The model is oscillated at an amplitude of about 2° and at frequencies from about 10 to 50 cycles per second. The sting mechanism provides changes in angle of attack while maintaining model position approximately on the wind-tunnel center line. All models were bodies of revolution and were built principally of brass and aluminum with aerodynamically smooth exposed surfaces. Dimensions of the various models are given in figure 2.

TESTS AND PROCEDURE

The tests were made at Mach numbers from 0.59 to 1.35 but no data are presented for Mach numbers where calculations, obtained by using the method of reference 6, predicted wall-reflected shock disturbances on the various models.

Tunnel stagnation pressures were about 30 and 60 pounds per square inch absolute with corresponding Reynolds numbers, based on maximum model diameters, varying from 1.8×10^6 to 5.6×10^6 (fig. 3).

For certain tests a transition strip of carborundum grains, 0.001 to 0.002 inch in diameter, was applied to the models according to the suggestions of reference 7. (See fig. 2 for location of transition strip.) The effect of roughness type was investigated for one of the models as explained subsequently in the section entitled "Effects of Model Surface Condition and Reynolds Number."

Measurements were made at $\alpha = 0^{\circ}$, 5°, and 10°. The reduced-frequency parameter $\omega d/V$ varied from 0.019 to 0.105. In operation of the oscillating balance and model system, calibrated outputs of the moment and displacement strain gages are passed through coupled electrical sine-cosine resolvers which rotate at the frequency of model oscillation. (See fig. 1(a).) The resolvers split up the moment and displacement signals into orthogonal components which are simultaneously read on damped direct-current microammeters. From these components the applied moment and displacement and the phase angle between them can be found. With these and the measured oscillation frequency, the system damping and oscillatory spring constants can be computed. The measured wind-off characteristics were subtracted from the wind-on system measurements to give the desired aerodynamic results. For maximum accuracy

of damping measurements, the tests were made at or near the natural frequency of the model system. (See refs. 3 and 4.) Tunnel Mach number, dynamic pressure, and Reynolds number were determined from continuous records indexed at the time each data point was taken.

ACCURACY

The ability of this forced-oscillation method to determine accurately the damping of the oscillating model system was verified by using eddy-current damping and free-decay methods as described in reference 3. A comparison between the results of the two methods is given in figure 4 for several values of damping-coil current.

The dynamic data presented in this paper were taken during two separate testing periods several months apart. Repeat test points checked very well except where the model flow conditions were critical and the measured moments were very dependent on the detailed flow over the model.

Where a definite flow condition was well established, the accuracy of determining the damping-in-yaw parameter was about ± 0.1 and the accuracy of determining the oscillatory-directional-stability parameter was about ± 0.01.

Mach number was accurate to ± 0.01, angle of attack to $\pm 0.1^{\circ}$, and unit Reynolds number to $\pm 0.1 \times 10^6$.

RESULTS AND DISCUSSION

Variations of the damping-in-yaw parameter $\left(C_{n_r} - C_{n_{\dot{\beta}}} \cos \alpha\right)_{\omega}$ and the oscillatory-directional-stability parameter $\left(C_{n_\beta} \cos \alpha + \left(\frac{\omega d}{V}\right)^2 C_{n_{\dot{r}}}\right)_{\omega}$ with Mach number for the models tested are presented in figures 5 to 12. Short discussions of the more important trends are presented in the following sections.

Effects of Shoulder Radius

For both the square- and round-shoulder cylinder bodies of fineness ratio 1 (models 100 and 110, respectively), the flow was apparently separated over the afterbody at subsonic speeds as pointed out in reference 1. This separated flow gave appreciable negative damping (fig. 5).

(Negative damping corresponds to a positive value of the damping-in-yaw parameter $\left(C_{n_r} - C_{n_{\dot{\beta}}} \cos \alpha\right)_{\omega}$.) Flow remained separated at supersonic speeds for the square-shoulder model but apparently expanded around the round-shoulder model and was attached to the afterbody giving positive damping. This is particularly noticeable at $\alpha = 0^{\circ}$. (Note the scatter in the data at subsonic speeds where the flow around the shoulder was critical.) For model 210 (fig. 6), with a converging body, the flow remained detached at supersonic speeds even with the round shoulder and produced the negative damping shown throughout the Mach number range. For model 310, which had a diverging body and round shoulder, the flow was attached throughout the Mach number range and gave positive damping. (See fig. 7.) The flow appeared to be partially separated at subsonic speeds for the square shoulder of model 300 and gave slight negative damping. The flow was attached for this model at supersonic speeds and resulted in positive damping similar to that of the round-shoulder model 310. (Again note the scatter in the data for the critical flow regions at subsonic speeds.)

Further evidence of this effect of separation on damping occurred for models 400 and 410, which are reentry bodies of higher fineness ratio. (See fig. 8.) At subsonic speeds and $\alpha = 0^{\circ}$, the separated flow caused zero or negative damping for both bodies. Model 400 with the square shoulder, had considerably greater negative damping than had model 410 with the round shoulder. Above sonic speeds the flow expanded around the shoulder and provided about the same measure of positive damping for both bodies.

For the several bodies just discussed, increased negative damping was accompanied by increased stability (a positive value of oscillatory-directional-stability parameter). Attached flow which provided the positive damping decreased the oscillatory-directional-stability parameter.

Effects of Angle of Attack

For the flat-face bodies, increase in angle of attack decreased the negative damping for test conditions with negative damping at $\alpha = 0^{\circ}$, and decreased the positive damping for conditions with positive damping at $\alpha = 0^{\circ}$. (See figs. 5 to 8.) This phenomenon is explained when it is considered that negative damping resulted from a separated flow region which was axially symmetric and shaped like a truncated cone. Increase in angle of attack caused the flow-cone to intersect the body on its lower surface and thus provided locally attached flow and a degree of positive damping. Conversely, for initially attached flow at $\alpha = 0^{\circ}$, increase in angle of attack caused an eventual separation on the upper surface with a decrease in total damping. Increase in angle of attack tended to decrease the oscillatory stability parameter although the effect is not pronounced. (Again, see figs. 5 to 8.)

Results at Sonic Speed

Sharp increases in negative damping near sonic speeds followed by an abrupt break to positive damping for supersonic speeds are noted for models 110 and 410 (figs. 5 and 8). A corresponding break in the oscillatory stability parameter is present. Similar trends in damping were found for similar bodies in wind-tunnel tests of reference 8, in free-flight tests of references 9, 10, and 11, and in ballistic-range tests of reference 12. Reference 8 considers this high negative damping to be the result of a hysteresis loop in the variation of moment with displacement angle. Since the static variation of moment with displacement angle was not determined in these tests, this hypothesis cannot be verified.

Effect of Center-of-Rotation Position

Tests of the effect of center-of-rotation position at $\alpha = 0^{\circ}$ were made with models 311, 312, and 313 (which are slightly larger versions of model 310) with diverging body slopes. No appreciable effects of center-of-rotation position are noted for the damping-in-yaw parameter (fig. 9). The portion of the damping contributed by loads on the face and base would be largely independent of longitudinal location of the center of rotation. Movement of the center of rotation rearward decreased the level of the oscillatory-directional-stability parameter for this shape; this decrease implies that the stability is a function of the longitudinal loading in phase with displacement.

Effects of Model Surface Condition and Reynolds Number

Model 510 is representative of a ballistic body of conical shape with a spherical segment nose. Damping of this model was positive at Mach numbers above 0.8 for all angles of attack (fig. 10). At Mach numbers less than 0.8, the flow was extremely critical and depended upon Reynolds number and the surface condition of the model nose. For the smooth condition, damping was negative at these subsonic speeds. Two-dimensional roughness in the form of a band of heavily distributed carborundum grains in glue did not affect the damping. A 1/10-inch-wide, 0.03-inch-thick "trip-ring" caused slight positive damping but did not produce the flow condition or the level of damping caused by the 1/10-inch-wide three-dimensional roughness strip in the form of carborundum grains, 0.001 to 0.002 inch in diameter, applied sparsely to the nose of the model according to the method of reference 7.

Increasing the Reynolds number for both the two- and three-dimensional roughness resulted in about the same increment of positive damping for these low Mach numbers.

The application of the trip-ring and three-dimensional roughness slightly increased the oscillatory-directional-stability parameter at subsonic speeds. At these lower Mach numbers increasing the Reynolds number increased the oscillatory-directional-stability parameter for the three-dimensional roughness condition only, while at supersonic speeds the increase in Reynolds number appeared to have no effect.

These important effects of test technique stress the fact that in dynamic testing of scale models of bodies of this sort, the full-scale flow condition, especially Reynolds number, must be reproduced. The aerodynamic damping of blunt bodies is very dependent upon detailed flow conditions over the body.

Effect of Body Base

Tests were made of model 510 with the original spherical segment base replaced with a flat base (model 500). Loads on the base of this body are obviously important inasmuch as the model with the flat base had about twice as much positive damping but half as much oscillatory stability in comparison with results with the model with the spherical-segment base (fig. 10). A similar effect on a body of this type was reported in reference 13.

Results for Specific Body Shapes

Model 600 (fig. 11), which is representative of a typical manned reentry body shape, showed moderately positive damping throughout the Mach number and angle-of-attack ranges and showed a very small value of positive stability. Doubling the Reynolds number at subsonic speeds showed no effect on either parameter.

Models 700 and 800, which were somewhat similar ballistic bodies, showed the significance of detailed differences. Model 700 in the smooth condition had moderate negative damping throughout the Mach number range (fig. 12). Application of roughness caused high negative damping subsonically and essentially zero damping supersonically. Doubling the Reynolds number for the rough model gave the same damping as for the smooth model at low Reynolds numbers. Damping-in-yaw and oscillatory-directional-stability parameters for model 800, on the other hand, were negligible for the test conditions.

Effect of Frequency on Stability

The static stability derivative C_{n_β}, as determined from the tests of reference 1, is compared with the oscillatory-directional-stability

parameter $\left(C_{n_\beta} \cos \alpha + \left(\frac{\omega d}{V}\right)^2 C_{n_{\dot{r}}}\right)_\omega$ in figure 13 for identical bodies. The good agreement between oscillatory and static data for models 110, 300, and 310, show that there was negligible frequency effect on the yaw stability derivatives. For model 210 of the present tests and model 9 of reference 1, there is some difference between levels of the static and oscillatory data although the trend with Mach number is similar. This difference in level is probably due to the effect of Reynolds number on the position of the flow separation although frequency effect may have caused some change.

CONCLUDING REMARKS

Transonic wind-tunnel tests were made to determine the damping-in-yaw and oscillatory-directional-stability parameters for models of various blunt, reentry shapes. Tests were made at Mach numbers of 0.59 to 1.35 and at angles of attack of 0°, 5°, and 10°. Reynolds number, based on maximum body diameter, varied from 1.8×10^6 to 5.6×10^6, and oscillation amplitude was about 2° for reduced-frequency parameters from 0.019 to 0.105.

Results show that the damping in yaw was critically dependent upon the detailed flow conditions over a blunt body. For flat-face bodies, negative damping resulted from separated flow on the afterbody whether caused by shoulder radius, body slope, Mach number, or angle of attack. Shape of the body base was important. The powerful influence of Reynolds number and type of transition roughness applied to some of the models emphasized that full-scale flow conditions must be reproduced closely for valid damping tests of blunt bodies. The oscillatory-directional stability was dependent upon the aforementioned factors but was not so critically affected as was the damping in yaw.

Langley Research Center,
National Aeronautics and Space Administration,
Langley Field, Va., June 29, 1960.

REFERENCES

1. Fisher, Lewis R., Keith, Arvid L., Jr., and DiCamillo, Joseph R.: Aerodynamic Characteristics of Some Families of Blunt Bodies at Transonic Speeds. NASA MEMO 10-28-58L, 1958.

2. Fisher, Lewis R., and DiCamillo, Joseph R.: Investigation of Several Blunt Bodies To Determine Transonic Aerodynamic Characteristics Including Effects of Spinning and of Extendible Afterbody Flaps and Some Measurements of Unsteady Base Pressure. NASA MEMO 1-21-59L, 1959.

3. Braslow, Albert L., Wiley, Harleth G., and Lee, Cullen Q.: Dynamic Directional Stability Derivatives for a 45° Swept-Wing—Vertical-Tail Airplane Model at Transonic Speeds and Angles of Attack, With a Description of the Mechanism and Instrumentation Employed. NACA RM L58A28, 1958.

4. Bielat, Ralph P., and Wiley, Harleth G.: Dynamic Longitudinal and Directional Stability Derivatives for a 45° Sweptback-Wing Airplane Model at Transonic Speeds. NASA TM X-39, 1959.

5. Burrows, Dale L., and Palmer, William E.: A Transonic Wind-Tunnel Investigation of the Force and Moment Characteristics of a Plane and a Cambered 3-Percent-Thick Delta Wing of Aspect Ratio 3 on a Slender Body. NACA RM L54H25, 1954.

6. Moeckel, W. E.: Approximate Method for Predicting Form and Location of Detached Shock Waves Ahead of Plane or Axially Symmetric Bodies. NACA TN 1921, 1949.

7. Braslow, Albert L., and Knox, Eugene C.: Simplified Method for Determination of Critical Height of Distributed Roughness Particles for Boundary-Layer Transition at Mach Numbers From 0 to 5. NACA TN 4363, 1958.

8. Reese, David E., Jr., and Wehrend, William R., Jr.: An Investigation of the Static and Dynamic Aerodynamic Characteristics of a Series of Blunt-Nosed Cylinder-Flare Models at Mach Numbers From 0.65 to 2.20. NASA TM X-110, 1960.

9. McFall, John C., Jr.: Dynamic Stability Investigation of Two Right Circular Cylinders in Axial Free Flight at Mach Numbers From 0.4 to 1.7 - Fineness Ratio-2.56 Cylinder and Fineness-Ratio-4.0 Cylinder With Flared Afterbody. NACA RM L56L28, 1957.

10. Coltrane, Lucille C.: Investigation of Two Bluff Shapes in Axial Free Flight Over a Mach Number Range From 0.35 to 2.15. NACA RM L58A16, 1958.

11. Coltrane, Lucille C.: Stability Investigation of a Blunt Cone and a Blunt Cylinder With a Square Base at Mach Numbers From 0.64 to 2.14. NACA RM L58G24, 1958.

12. Tom, William S.: Aerodynamic Characteristics of the ML-404-20 Polaris Re-Entry Models; Preliminary Results. Tech. Note 5034-32, U.S. Naval Ordnance Test Station (China Lake, Calif.), Nov. 14, 1957.

13. Wehrend, William R., Jr., and Reese, David E., Jr.: Wind-Tunnel Tests of the Static and Dynamic Stability Characteristics of Four Ballistic Re-Entry Bodies. NASA TM X-369, 1960.

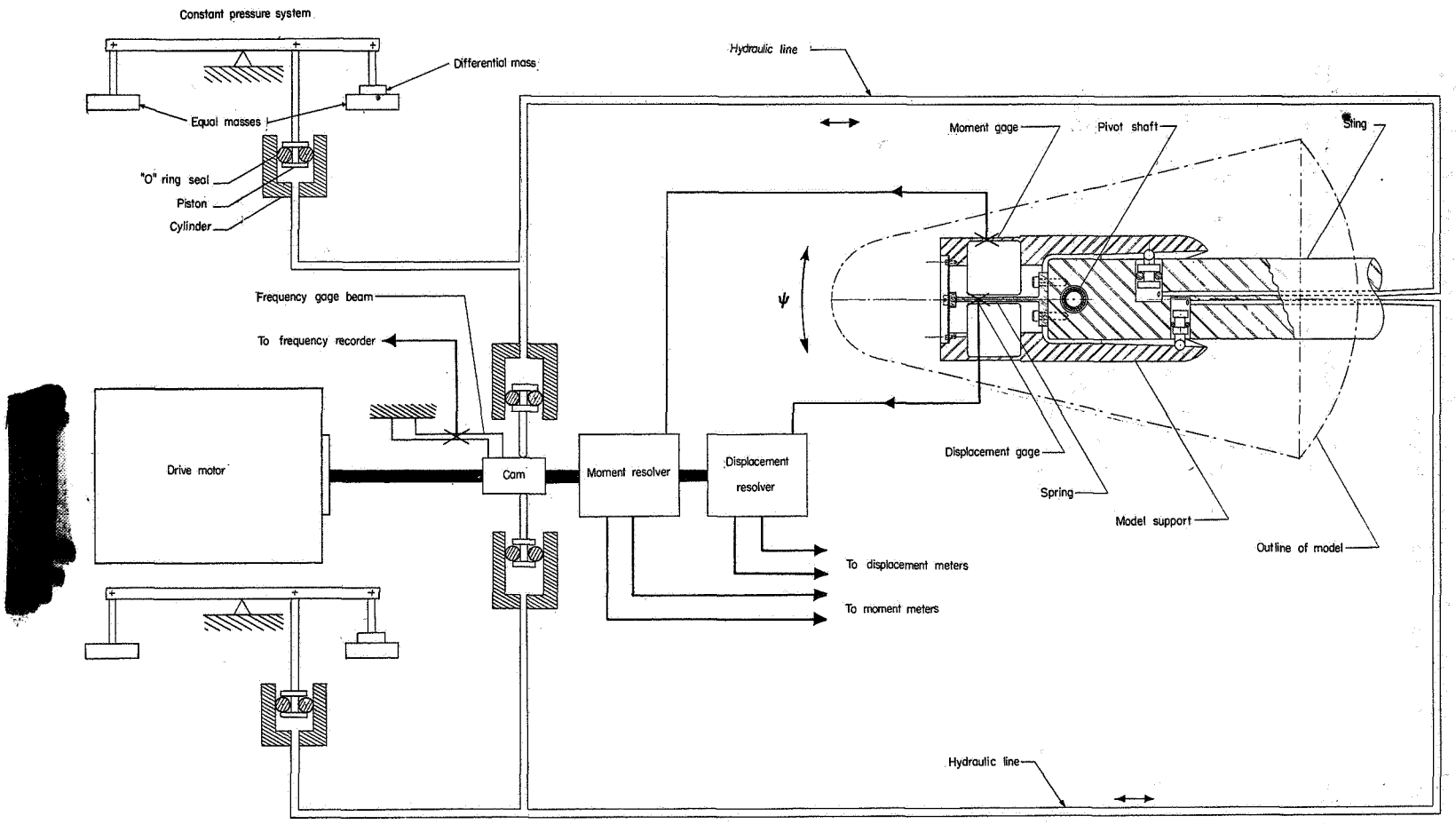

(a) Sketch of mechanism.

Figure 1.- Oscillating model mechanism.

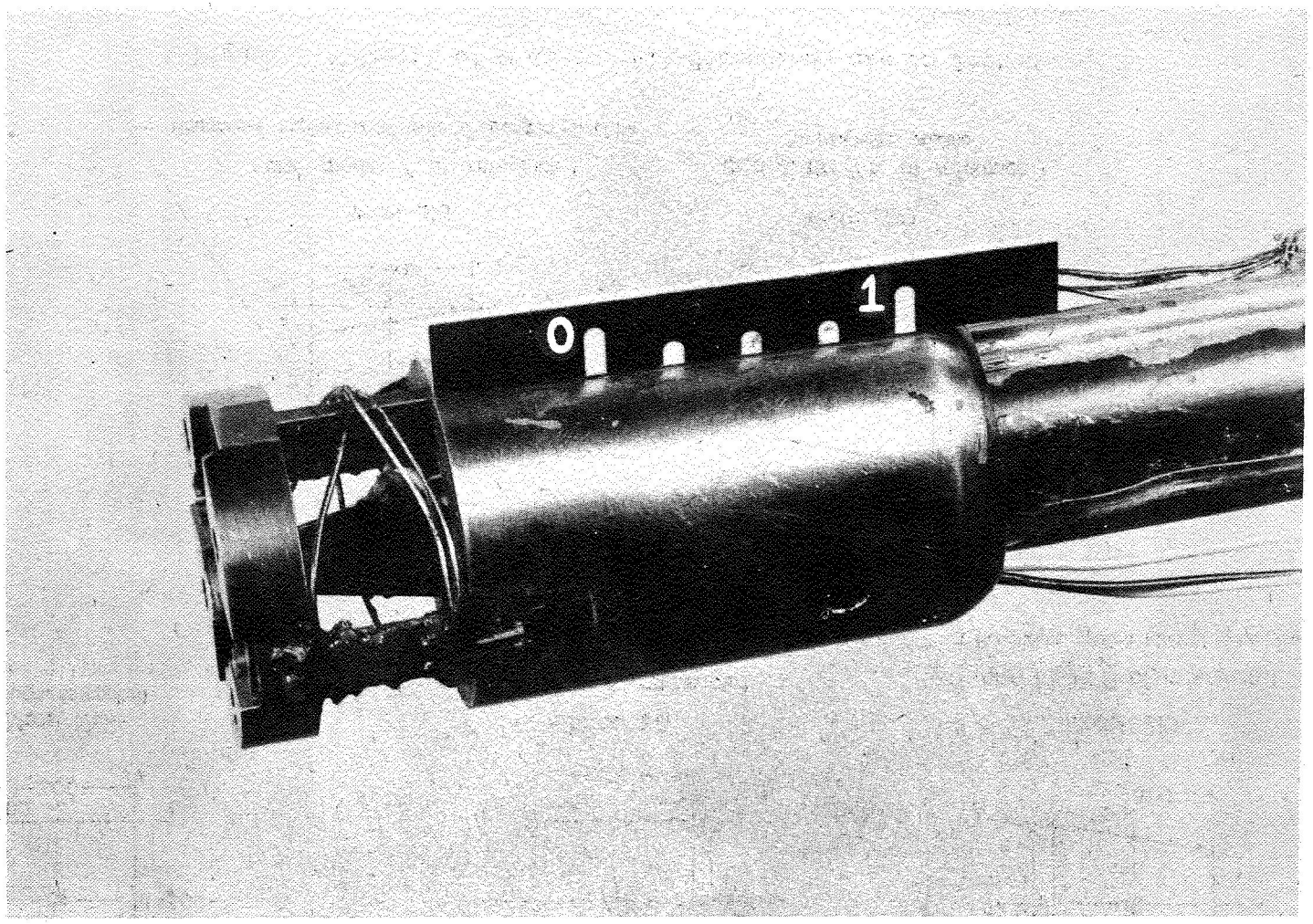

(b) Photograph of model support balance. L-58-717.1

Figure 1.- Concluded.

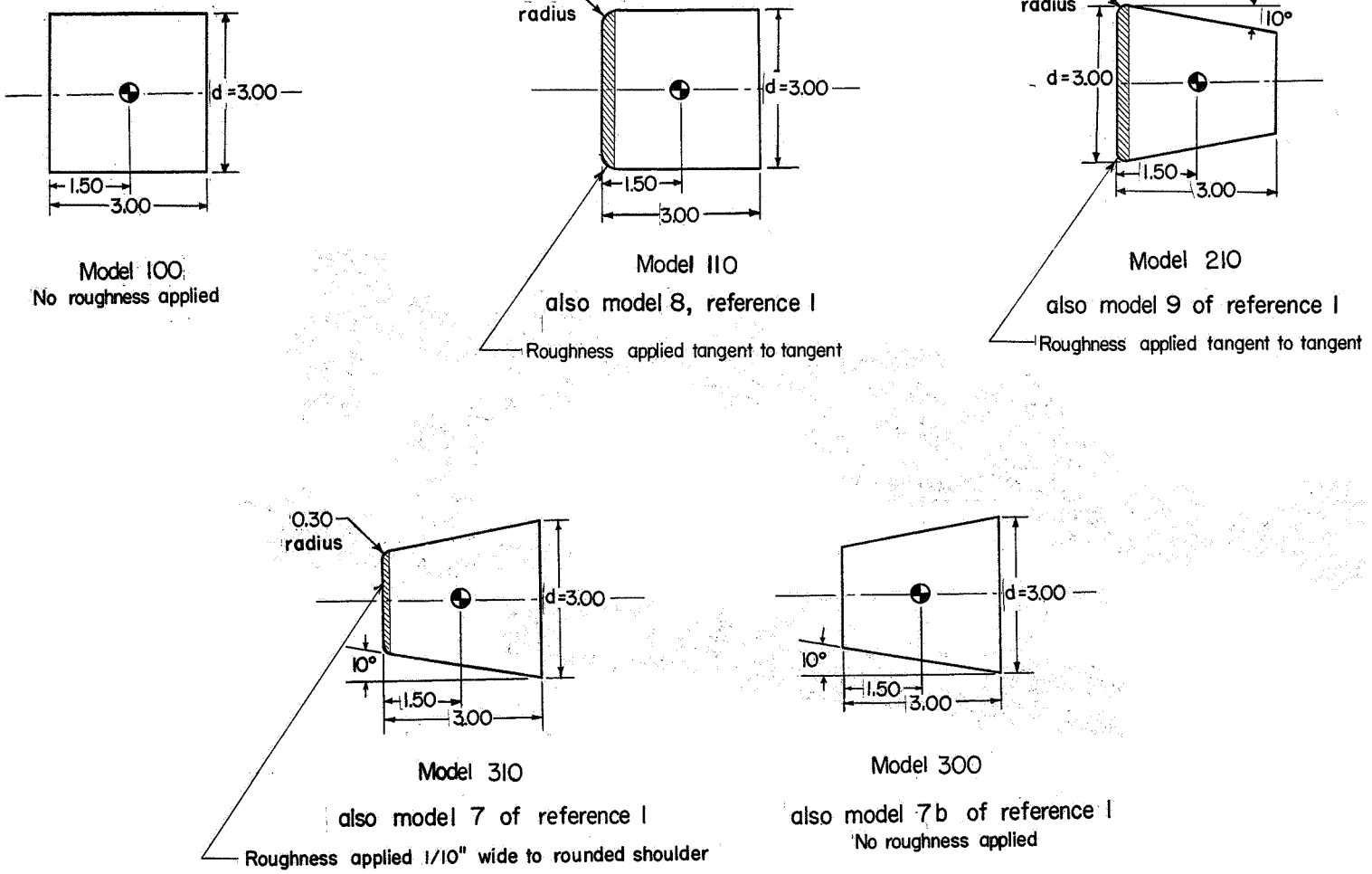

Figure 2.- Sketch of models. All dimensions are in inches.

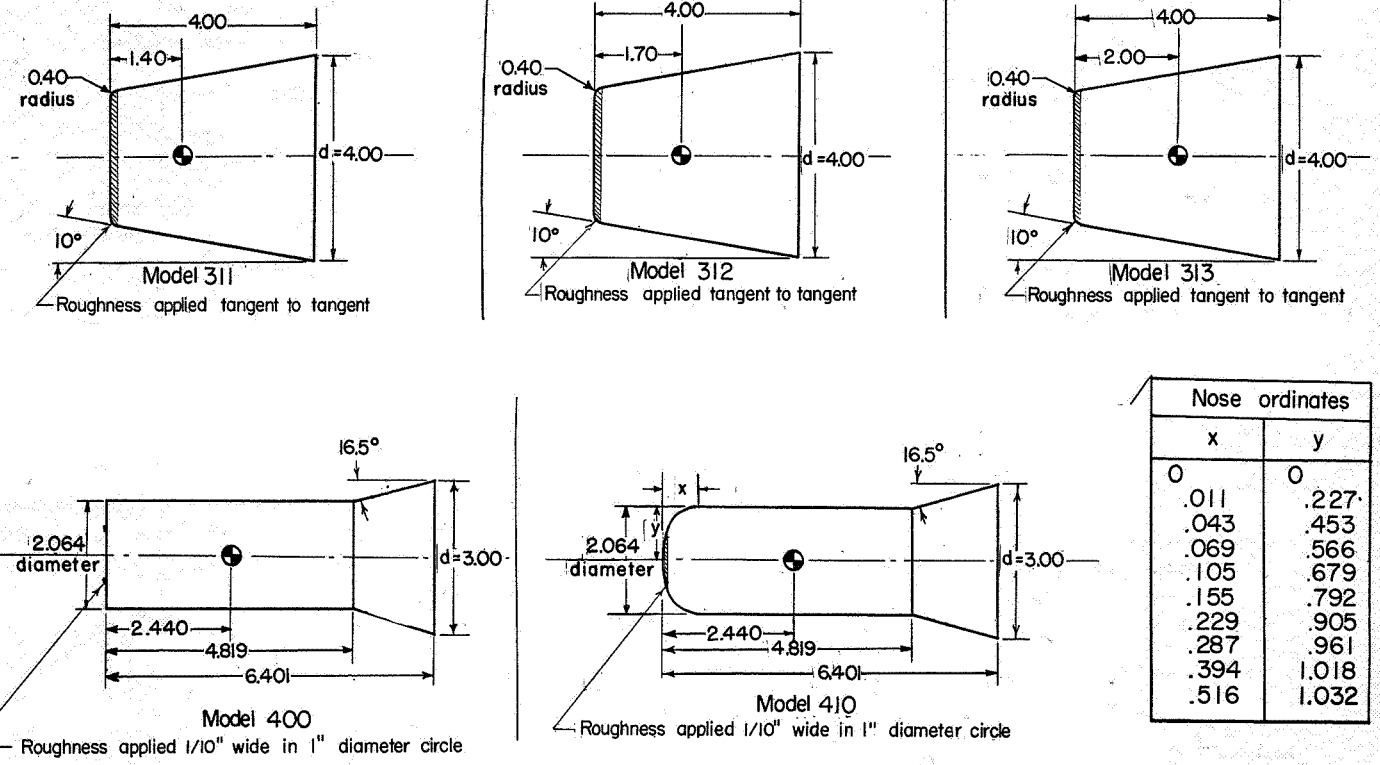

Nose ordinates

x	y
0	0
.011	.227
.043	.453
.069	.566
.105	.679
.155	.792
.229	.905
.287	.961
.394	1.018
.516	1.032

Figure 2.- Continued.

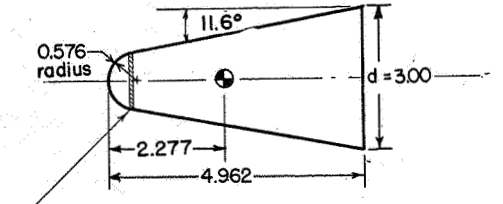

Model 500

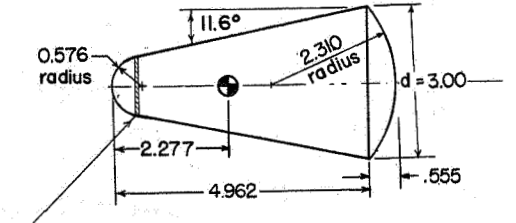

Model 510

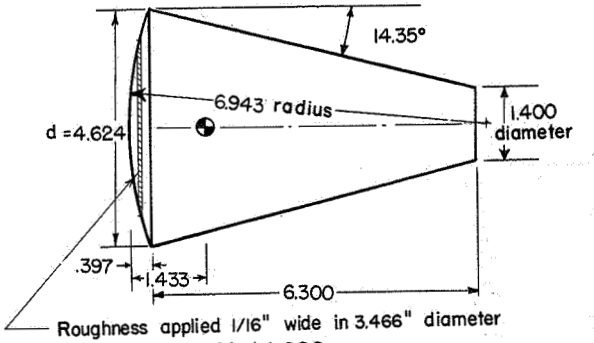

Model 600

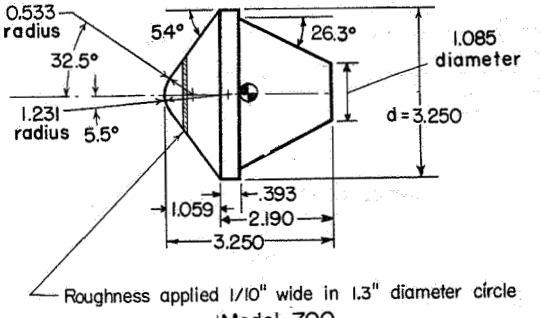

Model 700

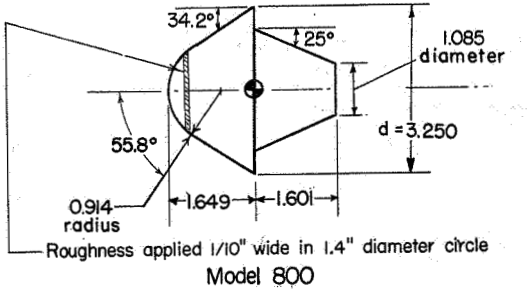

Model 800

Figure 2.- Concluded.

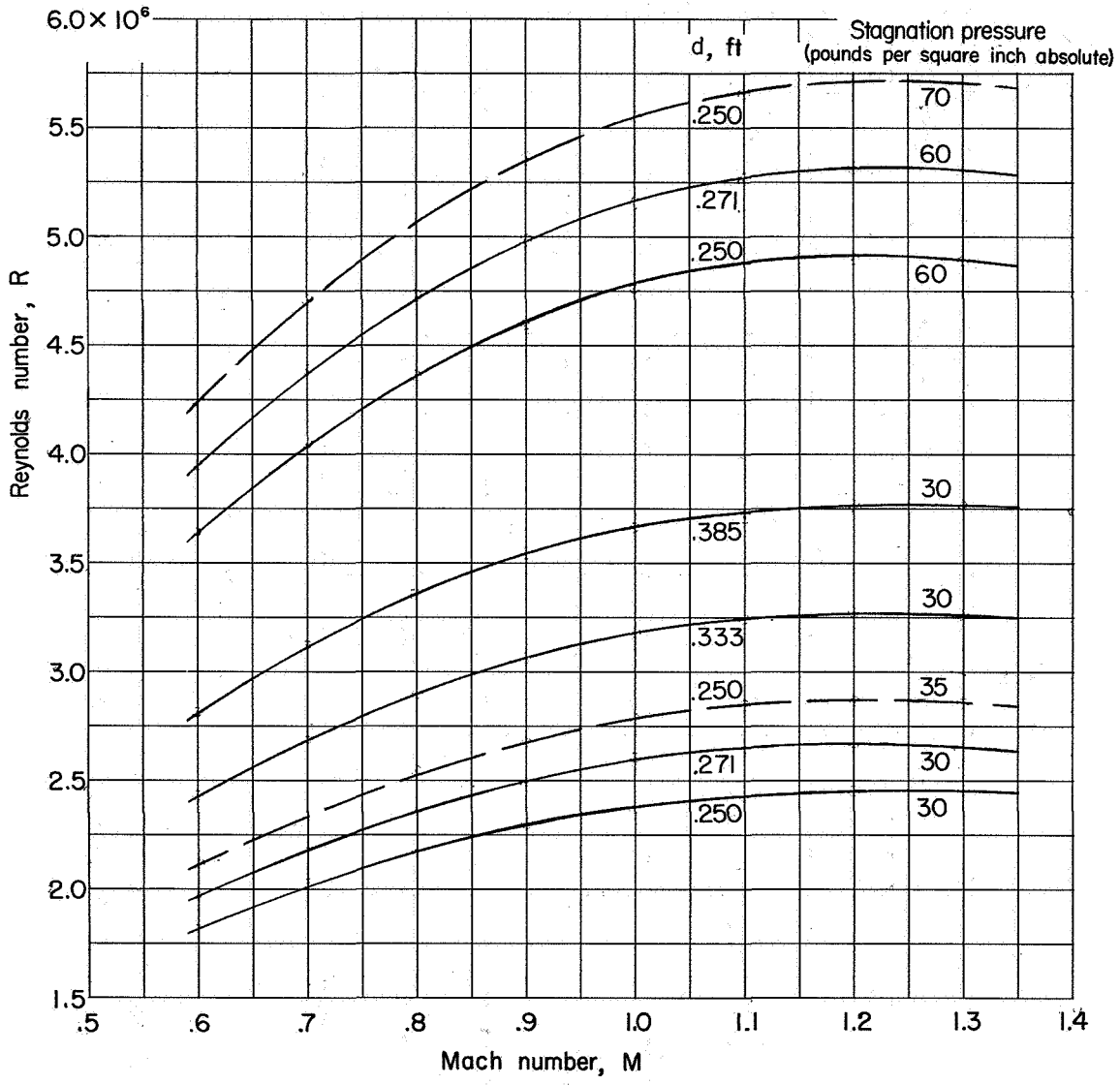

Figure 3.- Variation of Reynolds number with Mach number for all models tested. Stagnation temperature, 70° F. (Dashed lines are for the models from ref. 1.)

[redacted]

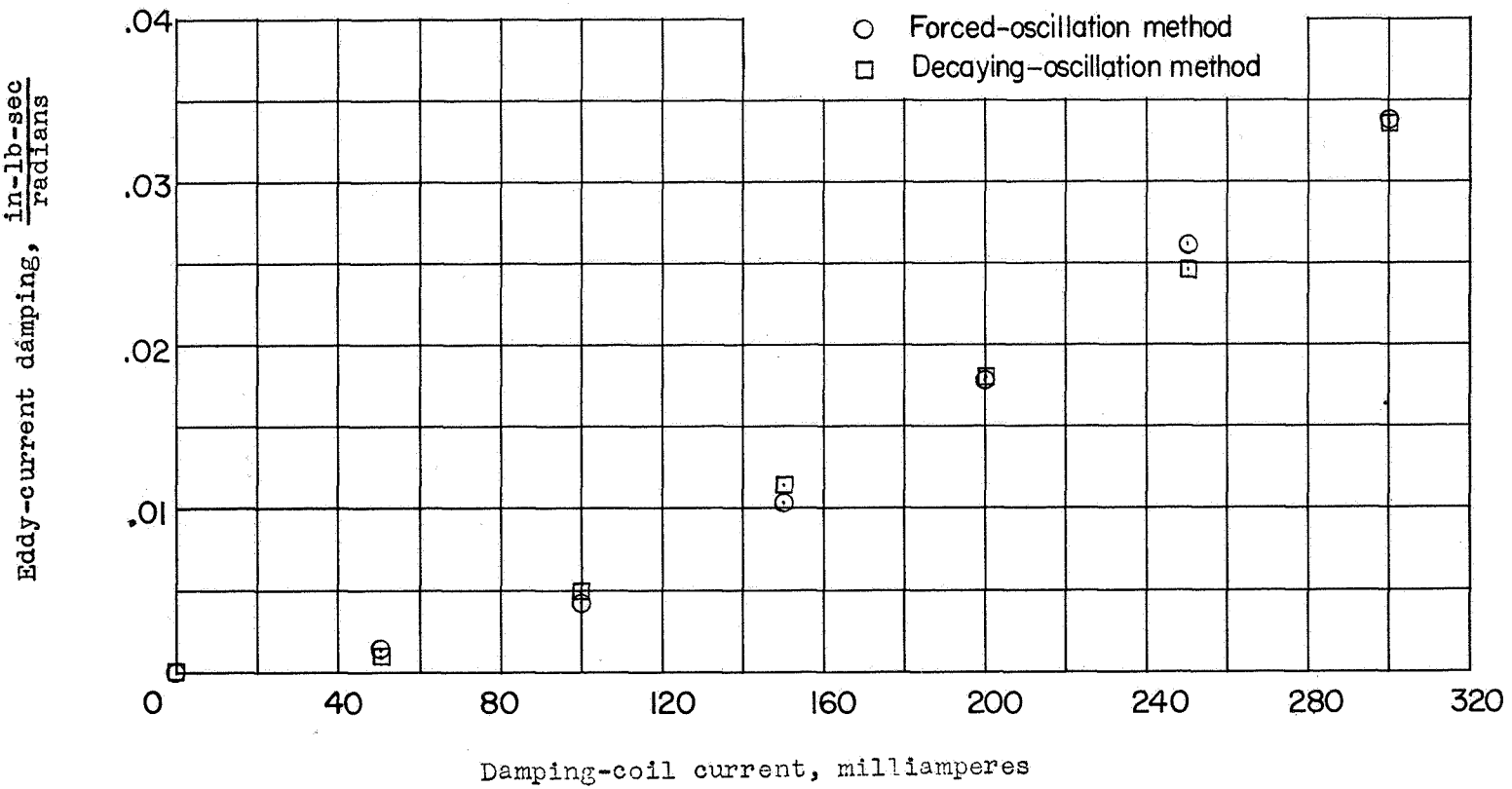

Figure 4.- Variation of measured eddy-current damping with damping-coil current as determined by the free-decay and force-driven techniques.

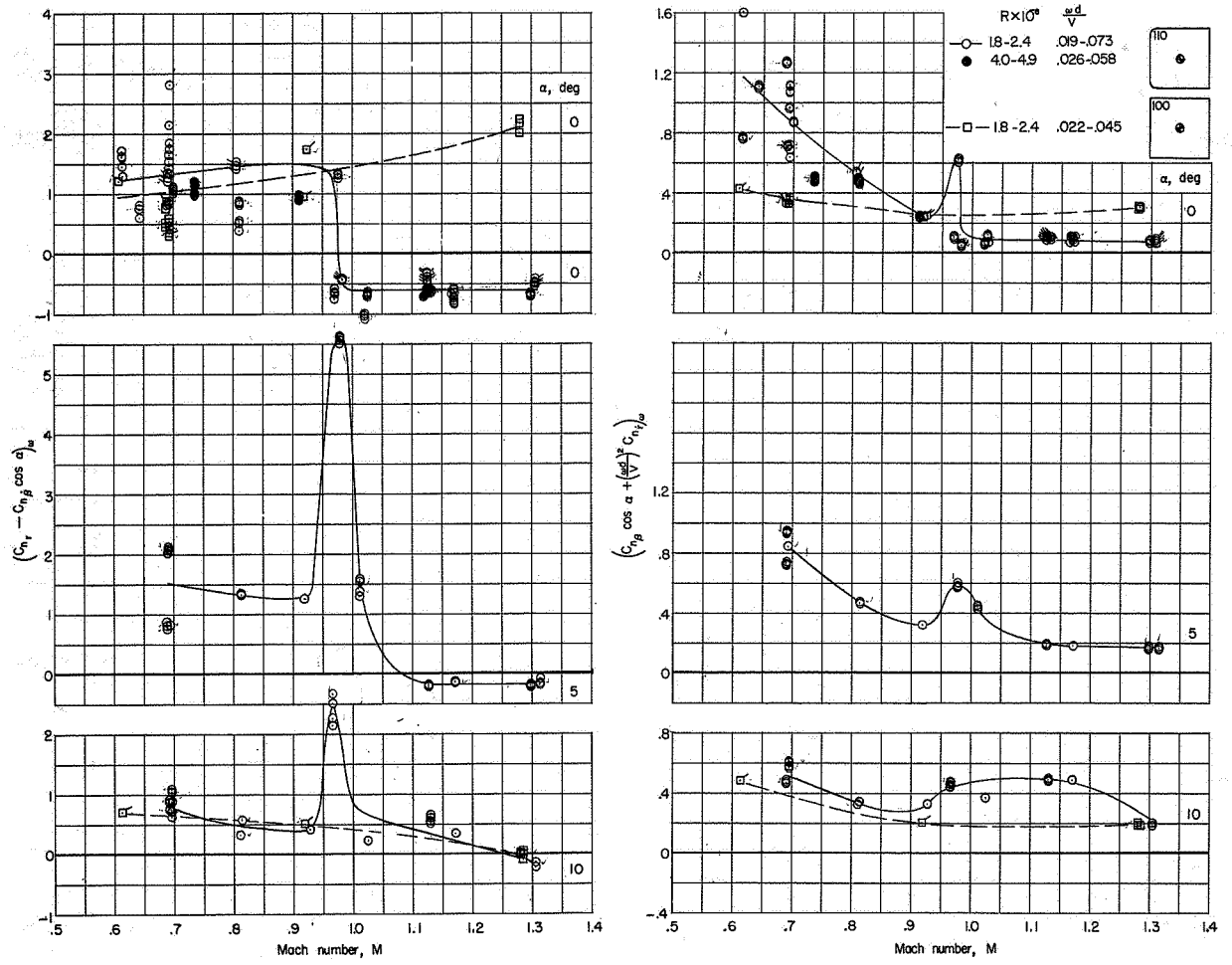

Figure 5.- The variation of $\left(C_{n_r} - C_{n_{\dot{\beta}}} \cos \alpha\right)_\omega$ and $\left(C_{n_\beta} \cos \alpha + \left(\frac{\omega d}{V}\right)^2 C_{n_{\dot{r}}}\right)_\omega$ with Mach number at various angles of attack for models 100 and 110 with and without roughness. Amplitude variation from 1.34° to 2.88°. (Flagged symbols indicate no roughness was applied.)

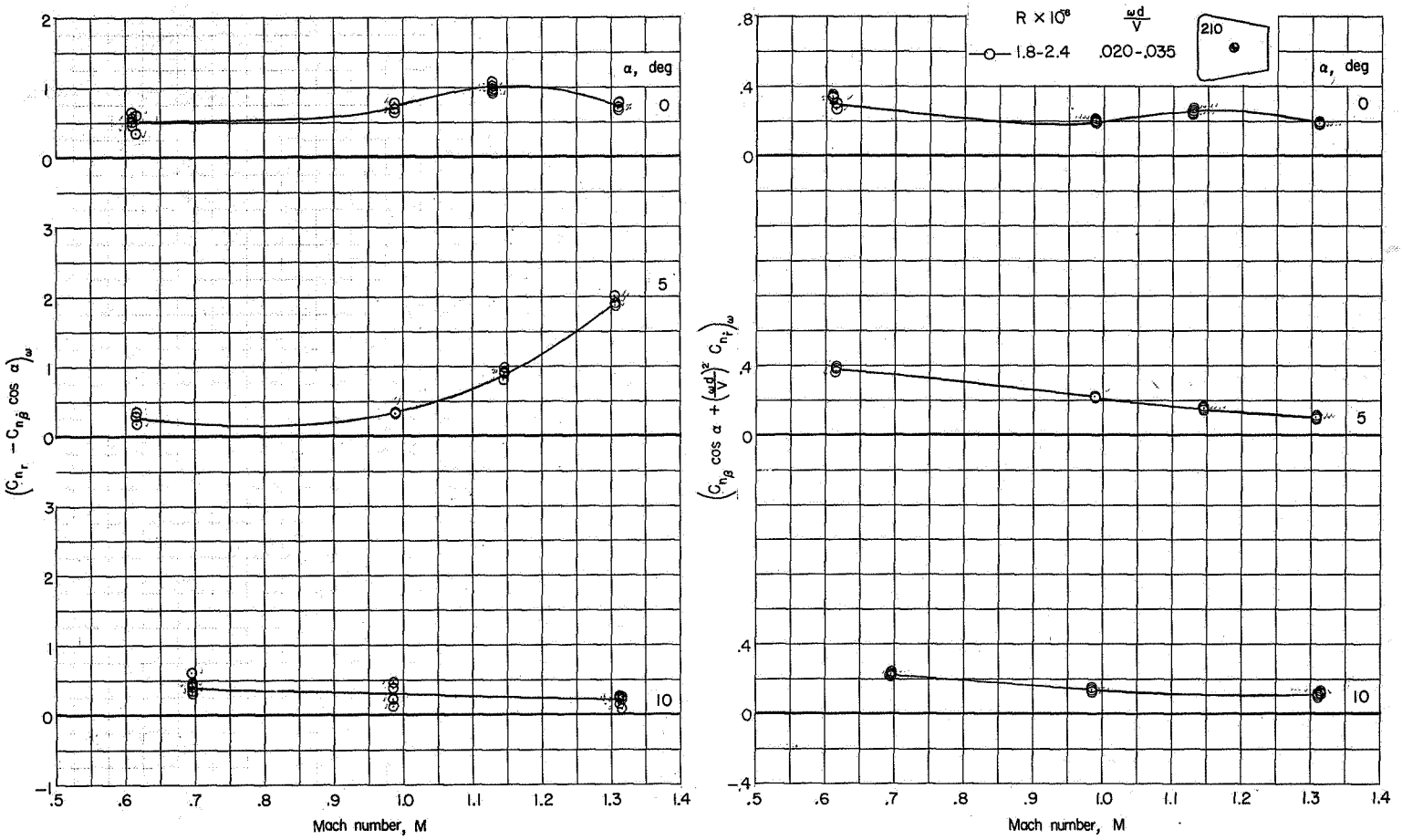

Figure 6.- The variation of $\left(C_{n_r} - C_{n_{\dot{\beta}}} \cos \alpha\right)_\omega$ and $\left(C_{n_\beta} \cos \alpha + \left(\frac{\omega d}{V}\right)^2 C_{n_{\dot{r}}}\right)_\omega$ with Mach number at various angles of attack for model 210 with roughness. Amplitude variation from 1.78° to 2.10°.

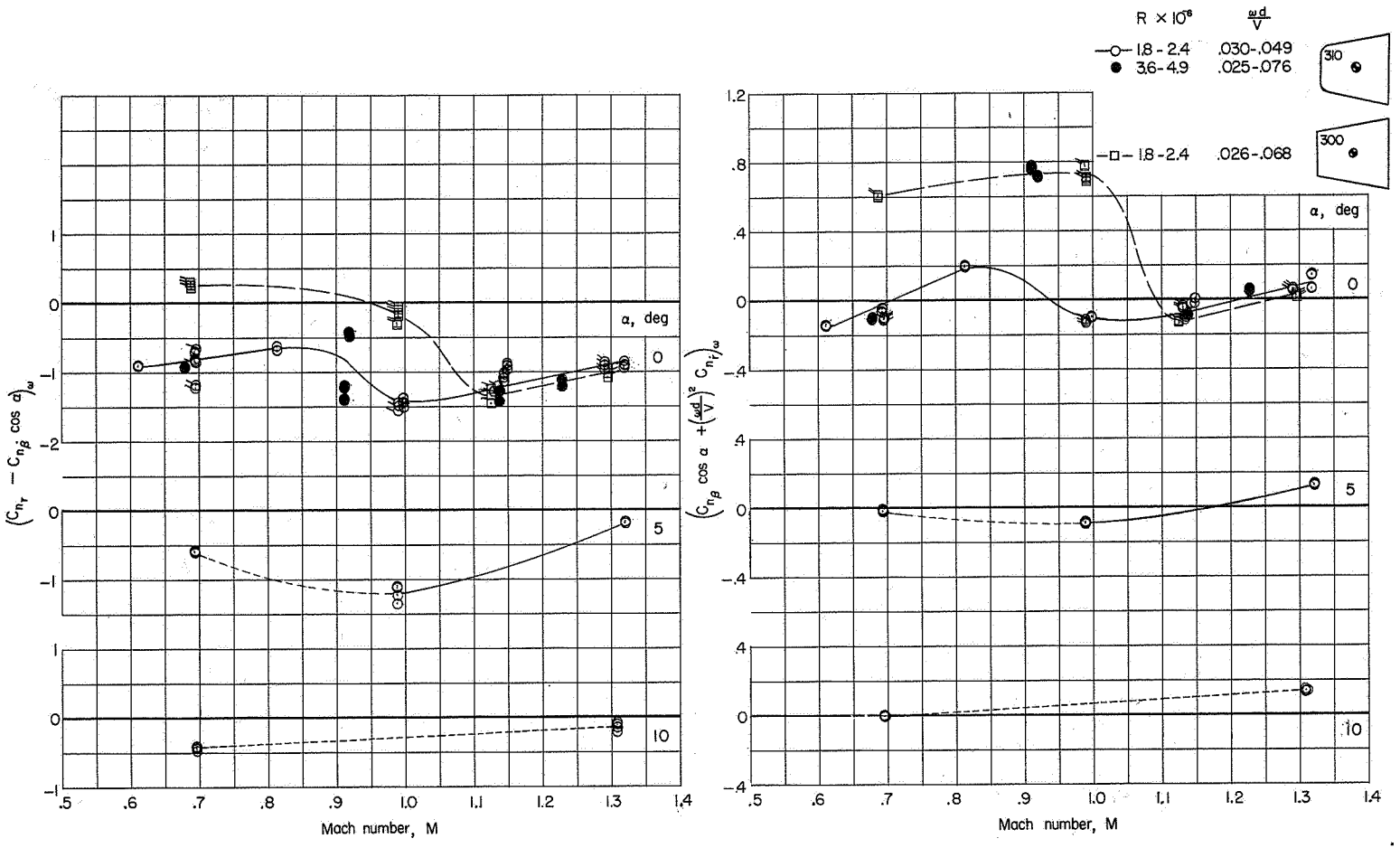

Figure 7.- The variation of $\left(C_{n_r} - C_{n_{\dot{\beta}}} \cos \alpha\right)_\omega$ and $\left(C_{n_\beta} \cos \alpha + \left(\frac{\omega d}{V}\right)^2 C_{n_{\dot{r}}}\right)_\omega$ with Mach number at various angles of attack for models 300 and 310 with and without roughness. Amplitude variation from 1.20° to 2.75°. (Flagged symbols indicate no roughness was applied.)

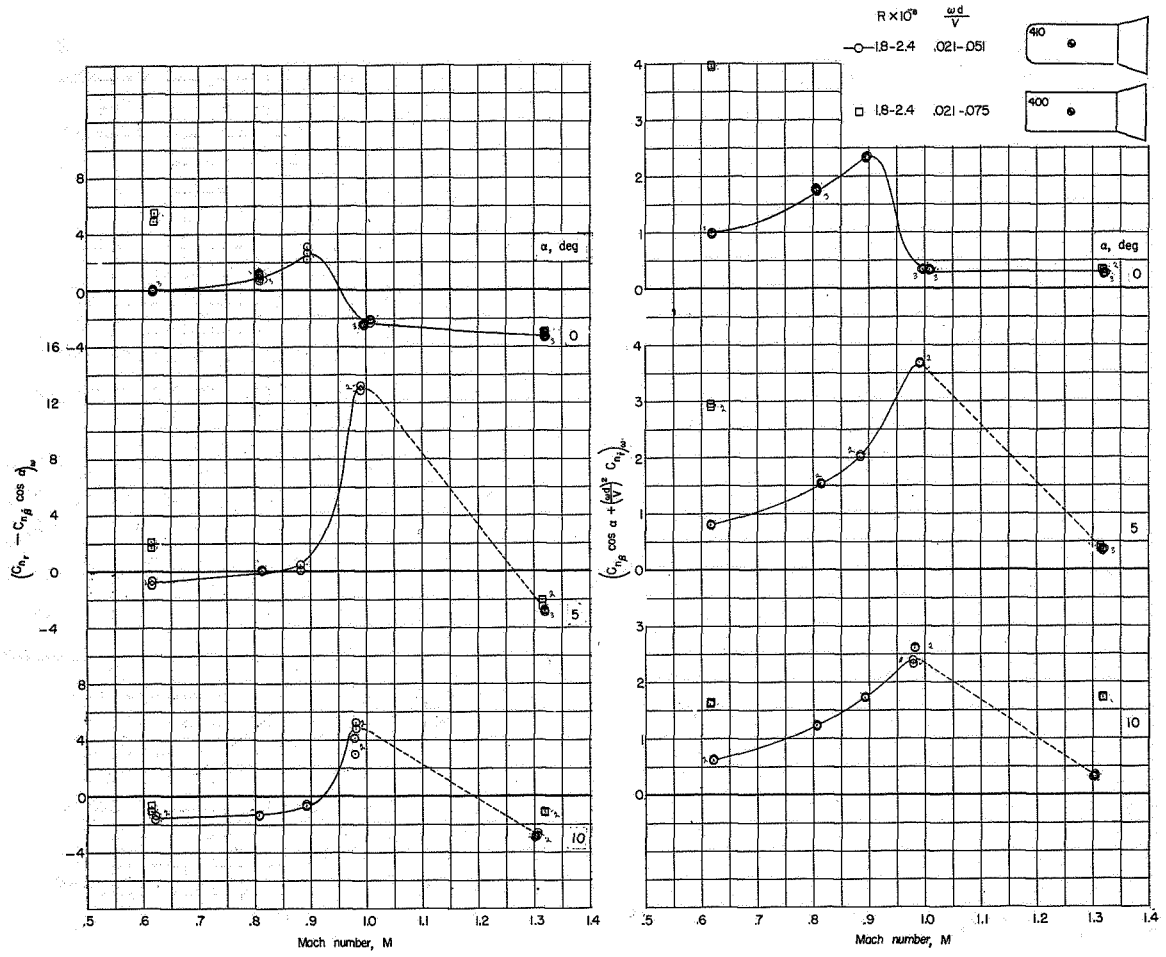

Figure 8.- The variation of $\left(C_{n_r} - C_{n_{\dot{\beta}}} \cos \alpha\right)_\omega$ and $\left(C_{n_\beta} \cos \alpha + \left(\frac{\omega d}{V}\right)^2 C_{n_{\dot{r}}}\right)_\omega$ with Mach number at various angles of attack for models 400 and 410 with roughness. Amplitude variation from 1.18° to 2.22°.

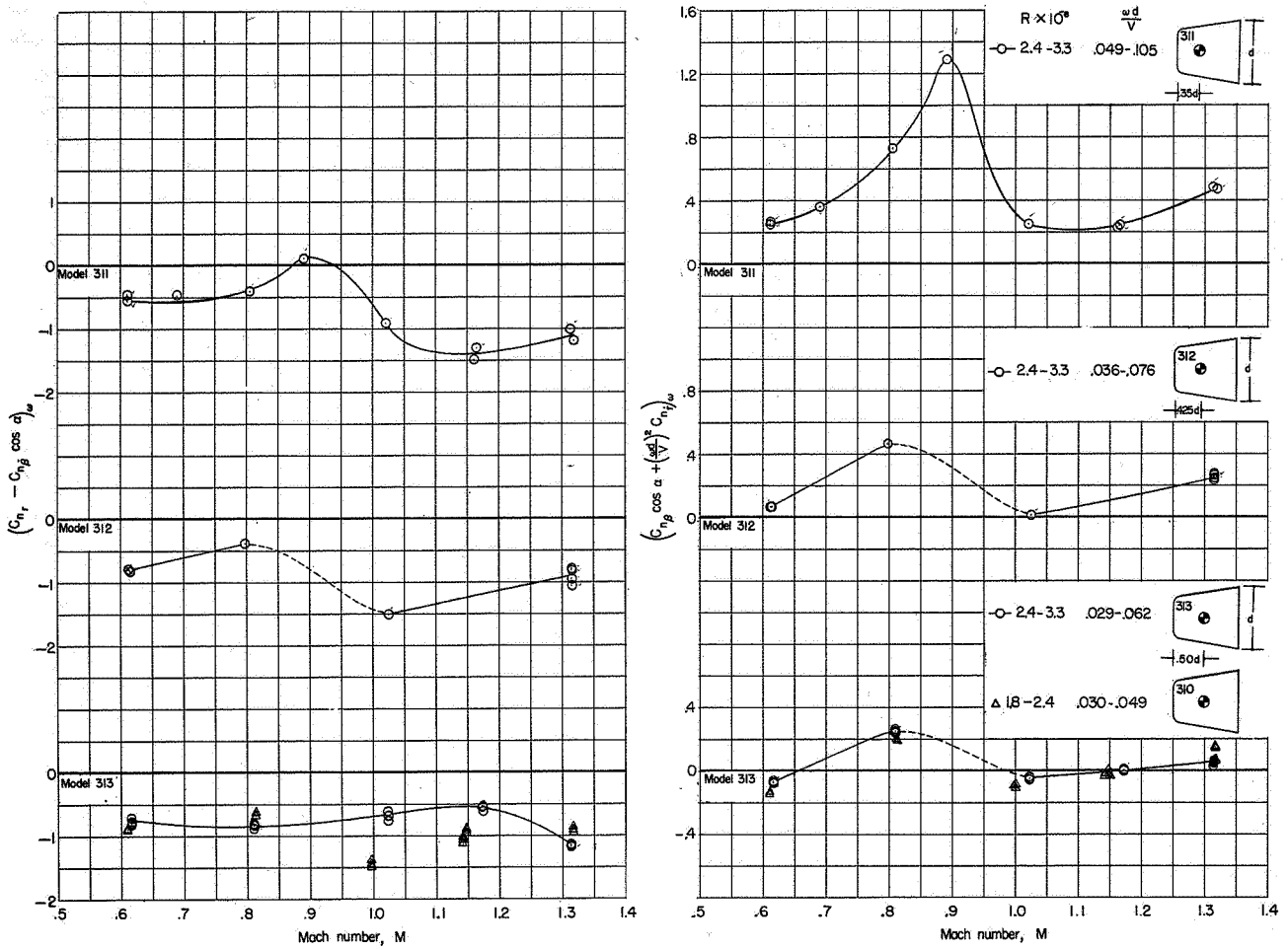

Figure 9.- The variation of $\left(C_{n_r} - C_{n_{\dot{\beta}}} \cos \alpha\right)_\omega$ and $\left(C_{n_\beta} \cos \alpha + \left(\frac{\omega d}{V}\right)^2 C_{n_{\dot{r}}}\right)_\omega$ with Mach number at $\alpha = 0^\circ$ for models 310, 311, 312, and 313 with roughness and with various center-of-rotation positions. Amplitude variation from 1.23° to 2.38°.

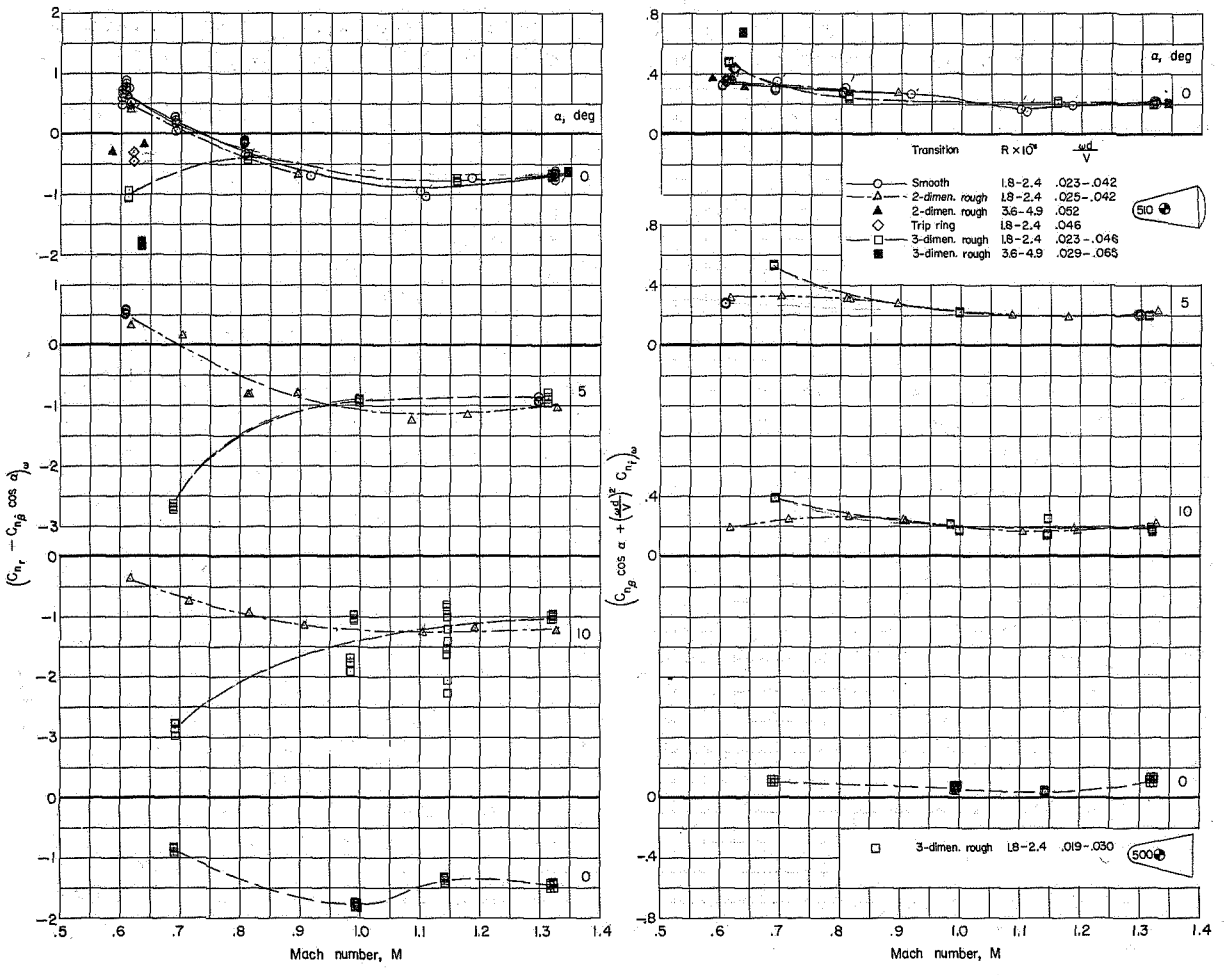

Figure 10.- The variation of $\left(C_{n_r} - C_{n_{\dot\beta}} \cos\alpha\right)_\omega$ and $\left(C_{n_\beta}\cos\alpha + \left(\frac{\omega d}{V}\right)^2 C_{n_{\dot r}}\right)_\omega$ with Mach number at various angles of attack for models 500 and 510 with various surface conditions. Amplitude variation from 1.86° to 2.46°.

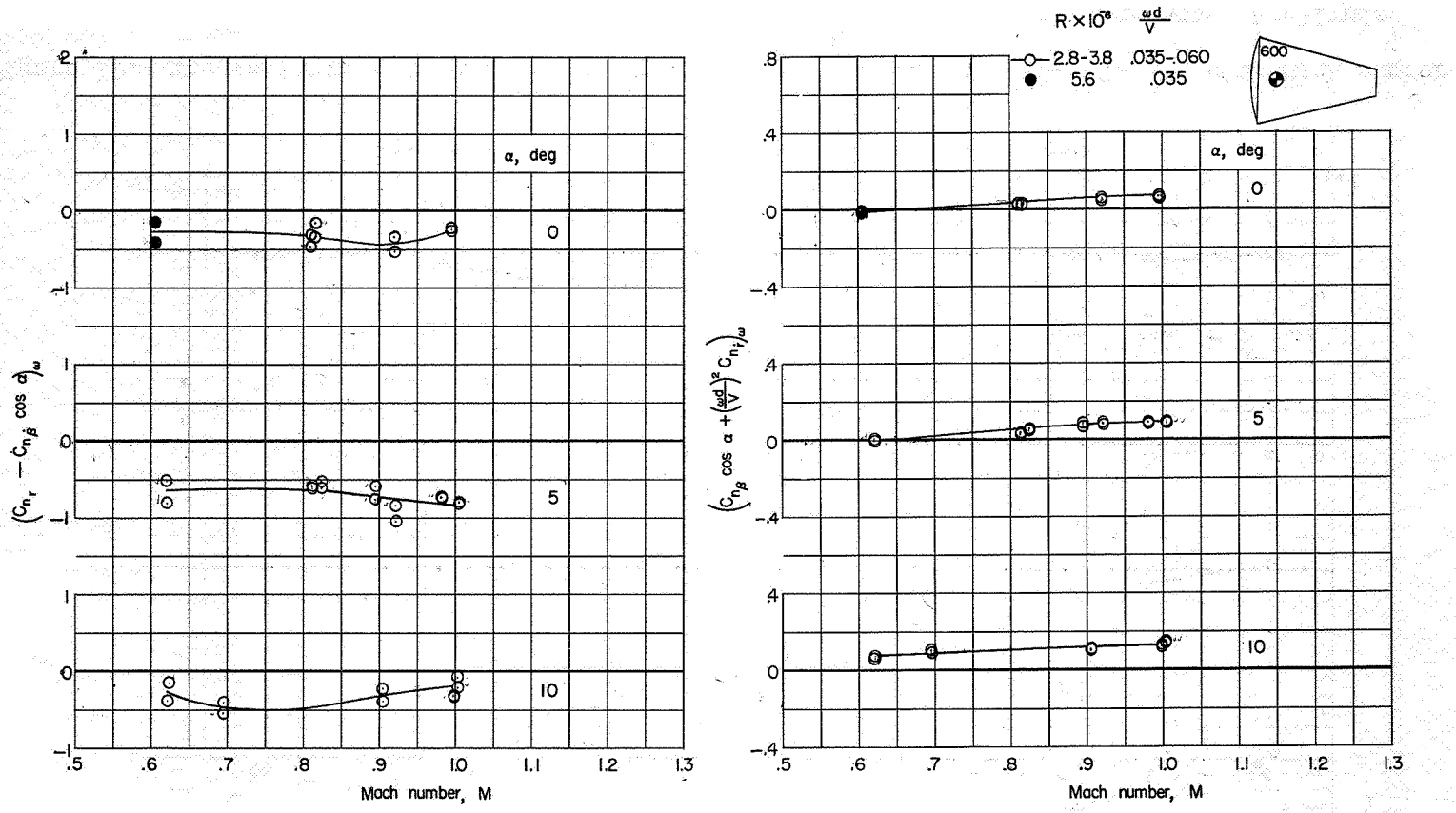

Figure 11.- The variation of $\left(C_{n_r} - C_{n_{\dot{\beta}}} \cos \alpha\right)_\omega$ and $\left(C_{n_\beta} \cos \alpha + \left(\frac{\omega d}{V}\right)^2 C_{n_{\dot{r}}}\right)_\omega$ with Mach number at various angles of attack for model 600 with roughness. Amplitude variation from 1.15° to 1.72°.

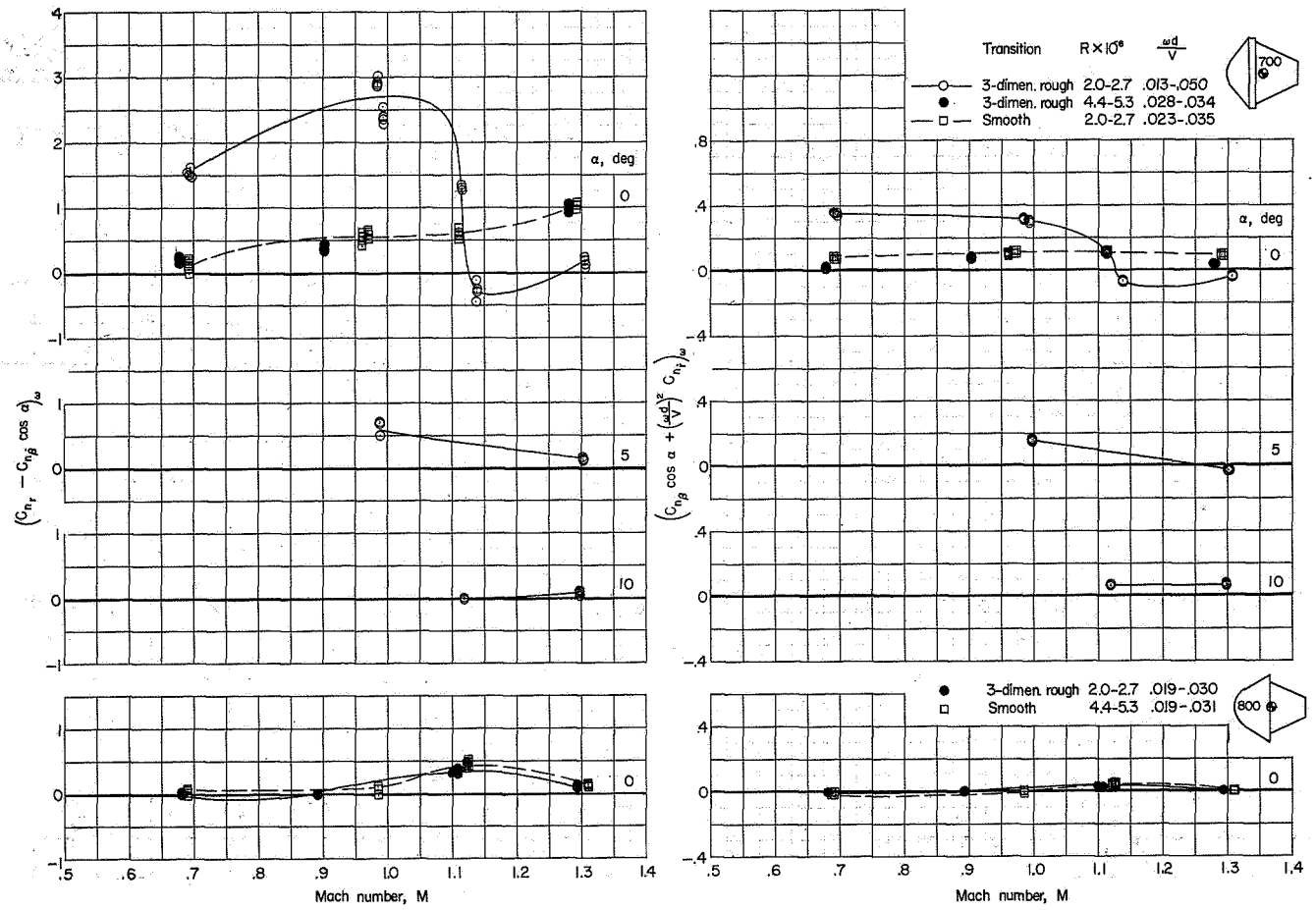

Figure 12.- The variation of $\left(C_{n_r} - C_{n_{\dot\beta}} \cos\alpha\right)_\omega$ and $\left(C_{n_\beta} \cos\alpha + \left(\frac{\omega d}{V}\right)^2 C_{n_{\dot r}}\right)_\omega$ with Mach number at various angles of attack for models 700 and 800 with and without roughness. Amplitude variation from 1.81° to 3.04°.

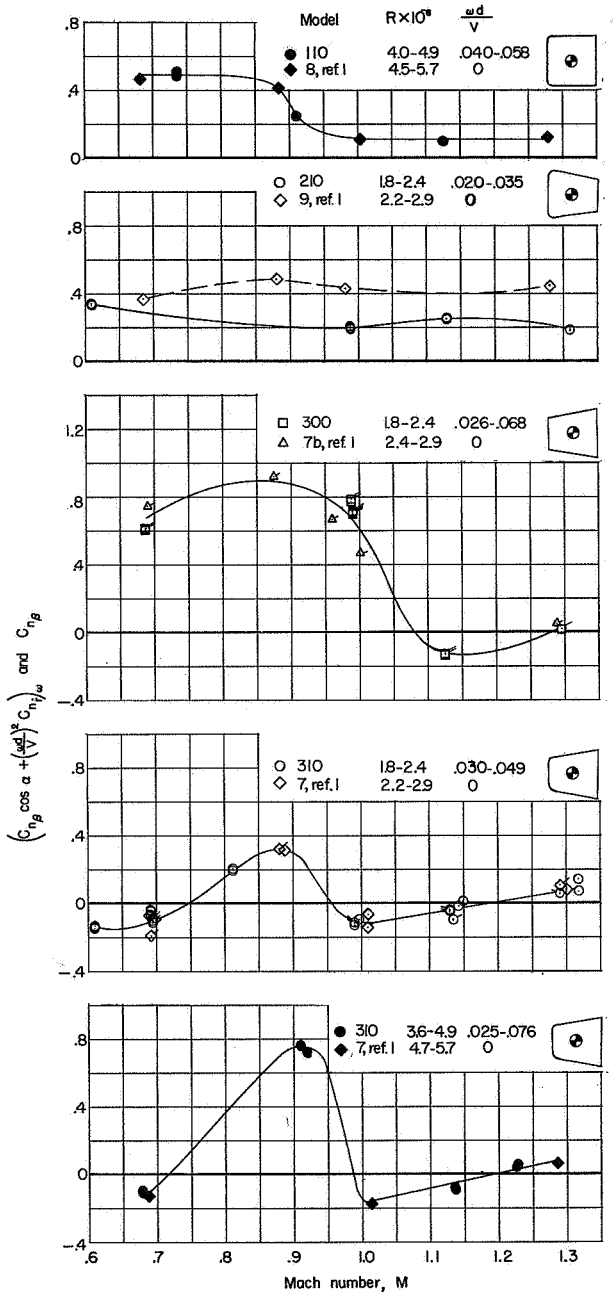

Figure 13.- The variation of C_{n_β} and $\left(C_{n_\beta}\cos\alpha+\left(\frac{\omega d}{V}\right)^2 C_{n_{\dot{r}}}\right)_\omega$ with Mach number at $\alpha = 0^\circ$ for models 110, 210, 300, and 310 with and without roughness. (Flagged symbols indicate no roughness was applied.)